FULL PAPER

Dalton
www.rsc.org/dalton

Syntheses, crystal structures, ferroelectrics and magnetic properties of $[R\text{-}BzPy]_2[Cu(mnt)_2]$ complexes ($[R\text{-}BzPy]^+$ = 1-(4′-R-benzyl)-pyridinium, R = NO_2 or Br; mnt^{2-} = maleonitriledithiolate)

Xiaoming Ren,[a,b] Jing Ma,[c] Changsheng Lu,[b] Senzu Yang,*[a] Qingjin Meng*[b] and Peiheng Wu*[a]

[a] *Department of Electronic Science & Engineering, Nanjing University, Nanjing, 210093, P. R. China*

[b] *Coordination Chemistry Institute, State Key Laboratory of Coordination Chemistry, Nanjing University, Nanjing, 210093, P. R. China*

[c] *Institute of Theoretical and Computational Chemistry, Nanjing University, Nanjing, 210093, P. R. China*

Received 21st October 2002, Accepted 14th February 2003
First published as an Advance Article on the web 24th February 2003

The structures of two ion-pair complexes, which consist of 1-(4′-R-benzyl)pyridinium (R = NO_2 (**1**), Br (**2**)) and bis(maleonitriledithiolato)cuprate(II), have been determined by X-ray single crystal analyses, and the results show the stacking patterns in **1** and **2** are different from each other although the difference between the molecular structures of these complexes is only the substituent of the benzene ring, which may arise from the difference of interactions between cations and anions in these two complexes. Complex **1** crystallizes in the non-centrosymmetric space group *P*1, and dielectric measurements shows ferroelectric behavior with a small hysteresis loop. Quantum chemistry calculation further indicate the electric dipole in a unit cell is 56.5509 Debye, and DSC analysis reveal a T_c of 377 K, from the paraelectric to the ferroelectric phase. The magnetic susceptibilities of these two complexes measured in the temperature range 1.8–260 K show an antiferromagnetic coupling feature between neighboring Cu(II) ions with $\theta = -0.580$ K for **1** and -2.167 K for **2**. The polycrystalline EPR spectra of the two complexes at room temperature are different from each other, characterized axial *g* tensors are $g_{\|}$ of 2.09, $g_{\perp}$ of 2.02 for **1**, and $g_{\|} = 2.05$, $g_{\perp} = 2.03$, $A_{\|} = 40.6 \times 10^{-4}$ cm^{-1} for **2**.

Introduction

Recently, one-dimensional (1-D) compounds have been attracting widespread attention because of their novel physical properties, such as Peierls transition, spin-Peierls transition, charge-density-wave (CDW) states, spin-density-wave (SDV) states, spin-charge separation states, molecular bistabilities, and molecular magnetic nanowire properties, *etc*.[1] Furthermore, more and more new effects found in 1-D spin systems have also stimulated theoretical investigations.[1d,j]

One of the most studied classes of 1-D transition metal complexes are salts containing containing the $[M(mnt)_2]^-$ (M = Ni(III), Pd(III) or Pt(III)) ion. In these compounds, the constituent planar molecule $[M(mnt)_2]^-$ forms a columnar stack structure, in which intermolecular d_{z^2} or π orbital interactions result in a 1-D electronic nature.[2–4] In general, the topology and size of the counter cation in $[M(mnt)_2]^-$ complexes may play an important role in controlling the stacking pattern of anions and cations. In current studies, we have developed a new class of $[R\text{-}BzPy]^+[Ni(mnt)_2]^-$ salts containing the $[Ni(mnt)_2]^-$ anion and derivatives of benzylpyridinium ($[R\text{-}BzPy]^+$) as building blocks to construct low-dimensional molecular solids, and some significant and interesting results are described:[5] (1) The structural feature of $[R\text{-}BzPy]^+[Ni(mnt)_2]^-$ is that well-separated anions and cations form a regular anion stacking column and cation stacking column, respectively, in which $[Ni(mnt)_2]^-$ anions stack along the direction of anion column to form a spaced 1-D magnetic chain of $S = 1/2$. (2) The topology and size of the $[R\text{-}BzPy]^+$ ion, which is related to the molecular conformation of the $[R\text{-}BzPy]^+$ ion, can be modulated by systematic variation of the substituents in the aromatic rings. Therefore, the stacking pattern of these complexes can be finely tuned through controlling the molecular conformation of the $[R\text{-}BzPy]^+$ ion. (3) These classes of $[Ni(mnt)_2]^-$ complexes are strongly correlated electron systems, and magnetic coupled interactions in these systems are very sensitive to intermolecular separations. A series of complexes may be obtained, which show almost the same stacking structures but slightly different intermolecular separations, leading to magnetic diversity, such as 1-D antiferromagnetic linear Heisenberg chain, canting antiferromagnet, 1-D ferromagnetic chain, singlet–triplet thermal excitation in dimers, and some complexes reveal an unusual phase transition similar to the Peierls or spin-Peierls transition. With the goal of getting further information concerning the influence of molar ratio of the anion to cation on the stacking pattern of these classes of ion-pair complexes, we have pursued the study of complexes consisting of planar $[Cu(mnt)_2]^{2-}$ anions and substituted benzylpyridinium to obtain two complexes. Of these, one crystallizes in a non-centrosymmetric space group. In this paper, we report the syntheses, crystal structures, magnetic properties and ferroelectric properties of these complexes.

Experimental

Materials

All chemicals and solvents were of reagent grade, and used without further purification. Disodium maleonitriledithiolate (Na_2mnt) was synthesized by a published procedure.[6a] 1-(4′-R-benzyl)pyridinium chloride ([R-BzPy]Cl, R = NO_2 or Br) were prepared by the literature method.[6b]

Preparation of complexes

$[NO_2\text{-}BzPy]_2[Cu(mnt)_2]$ (1). An MeOH solution of Na_2mnt (372 mg, 2.0 mmol) was mixed with an MeOH solution of $CuCl_2 \cdot 2H_2O$ (171 mg, 1.0 mmol), stirred for 30 min at room temperature and filtered. A dark-red precipitate formed after adding a MeOH solution containing $[NO_2\text{-}BzPy]Cl$ (502 mg, 2.0 mmol) to the filtrate, which was filtered off, washed with MeOH, and then dried in vacuum. The crude product was dis-

DOI: 10.1039/b210314a

Table 1 Crystal data and structure refinement for **1** and **2**

Complex	**1**	**2**
Empirical formula	$C_{32}H_{22}CuN_8O_4S_4$	$C_{32}H_{22}Br_2CuN_6S_4$
Formula weight	774.36	842.16
Temperature/K	293(2)	293(2)
Wavelength/Å	0.71073	0.71073
Crystal system	Triclinic	Triclinic
Space group	$P1$	$P\bar{1}$
Unit cell dimensions		
a/Å	6.9660(14)	11.136(2)
b/Å	10.574(2)	11.884(2)
c/Å	12.026(2)	14.756(3)
α/°	72.84(3)	87.11(3)
β/°	85.48(3)	69.93(3)
γ/°	78.49(3)	65.14(3)
V/Å^3	829.2(3)	1654.1(6)
Z	1	2
D_c/Mg m^{-3}	1.551	1.691
Absorption coefficient/mm^{-1}	0.962	3.362
F(000)	395	838
Crystal size/mm	0.32 × 0.26 × 0.22	0.40 × 0.35 × 0.26
θ Range for data collection/°	1.77–24.97	1.48–24.97
Index ranges, hkl	0–8, −12 to 12, −14 to 14	0–13, −12 to 14, −16 to 17
Reflections collected	3138	6126
Independent reflections (R_{int})	3138 (0.0000)	5800 (0.0337)
Completeness to θ = 24.97° (%)	98.8	100.0
Absorption correction	ψ-Scan	ψ-Scan
Refinement method	Full-matrix least squares on F^2	Full-matrix least squares on F^2
Data/restraints/parameters	3138/3/442	5800/0/406
Goodness-of-fit on F^2	1.057	1.093
Final R indices [$I > 2\sigma(I)$]	$R1$ = 0.0339, $wR2$ = 0.0907	$R1$ = 0.0452, $wR2$ = 0.0987
R indices (all data)	$R1$ = 0.0413, $wR2$ = 0.0958	$R1$ = 0.1269, $wR2$ = 0.1184
Largest diff. peak and hole/e Å^{-3}	0.375 and −0.517	0.505 and −0.455

solved in 20 cm^3 MeCN and dark-red microcrystals were obtained by diffusing Et_2O (80 cm^3) into the solution. Yield: 627.4 mg (87%) (Found: C, 49.6; H, 2.93; N, 14.4. Calc. for $C_{32}H_{22}CuN_8O_4S_4$: C, 49.6; H, 2.86; N, 14.5%). IR bands of ν(C≡N) for mnt^{2-} (cm^{-1}): 2217.4 (sh), 2190.4s and 2160.4 (sh).

[BrBzPy]$_2$[Cu(mnt)$_2$] (2). This complex was prepared in similar way to that of **1**. Yield *ca.* 85% (Found: C, 45.4; H, 2.75; N, 9.86. Calc. for $C_{32}H_{22}Br_2CuN_6S_4$: C, 45.6; H, 2.63; N, 9.98%). IR bands of ν(C≡N) for mnt^{2-} (cm^{-1}): 2219.6 (sh), 2188.8s, 2154.1 (sh).

Physical measurements

Elemental analyses were performed with a Perkin-Elmer 240 analytical instrument. IR spectra were carried on an IFS66V FT-IR spectrophotometer in the region 400–4000 cm^{-1}. A RT6000 tester, working in the standard model, was used to measure the dielectric hysteresis loop at a frequency of 5 kHz on a single crystal 0.5 mm thick and 2.0 mm^2 in area deposited with platinum electrodes. DSC experiments were performed with a Perkin-Elmer calorimeter. Thermal analysis of polycrystalline samples placed in an aluminum crucible was carried with a heating rate of 20 K min^{-1} in the temperature range 323–443 K (50–170 °C). Magnetic susceptibilities were measured on a MagLab system 2000 magnetometer. EPR spectra at room temperature were recorded on a Bruker EMX X-band spectrometer operating at 100 kHz field modulation. The microwave frequency was calibrated using a frequency fitted in the microwave bridge ER 041 XG-D. Variable-temperature powder X-ray patterns were measured by a modified Guinier technique[7] (detection with image of plates, Fuji Bas-5000) using a capillary, with Cu-Kα radiation in the temperature range 299–389 K (26–116 °C).

Structure determinations of 1 and 2

Single crystals suitable for X-ray structure analysis were obtained by cooling MeCN solutions of complexes **1** and **2**. Single crystals of **1** and **2** were placed on a CAD4 diffractometer. Intensity data were collected at room temperature using graphite monochromated Mo-Kα radiation (λ = 0.71073 Å). The structure were solved by direct methods and refined on F^2 by full-matrix least-square methods using SHELXTL.[8] The crystal data collection and refinement parameters for **1** and **2** are summarized in Table 1.

CCDC reference numbers 169994 and 193971.

See http://www.rsc.org/suppdata/dt/b2/b210314a/ for crystallographic data in CIF or other electronic format.

Results and discussion

Descriptions of the structure of 1 and 2

[NO$_2$-BzPy]$_2$[Cu(mnt)$_2$] (1). The structure of **1** was determined by single crystal X-ray crystallography (Fig. 1). This is a structure with crystallographic imposed $P1$ symmetry. The Cu atom is coordinated by four S atoms of mnt^{2-} ligands in a [Cu(mnt)$_2$]$^{2-}$ anion, and shows deviation from the least-square

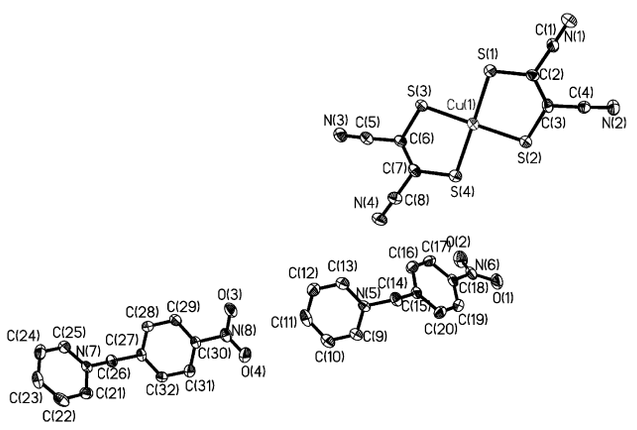

Fig. 1 ORTEP view and atomic labeling of **1** with 30% probability ellipsoids (H atoms omitted for clearity)

plane (S_4 plane) of 0.015 Å. The average Cu–S bond length is 2.27 Å, and the two S–Cu–S bond angles within the five-membered rings, S(2)–Cu(1)–S(3) 91.19(7)° and S(1)–Cu(1)–S(4) 90.94(7)°, are close to 90°, similar to that of a similar complex.[9] The $[Cu(mnt)_2]^{2-}$ anion exhibits a planar structure, while the N(1) atom of the CN group is displaced from the S_4 plane by 0.128 Å. There are two chemically equivalent but crystallographic distinct $[NO_2\text{-}BzPy]^+$ cations in the unit cell, A (containing N(5)) and B (containing N(7)). Both bond lengths and angles within A and B are almost identical, but the molecular conformations are different. The dihedral angles of the pyridine ring and benzene ring relative to the reference plane C_{Ar}–CH_2–C_{Py} are 108.9, 98.2° in A *cf.* 96.6, 114.0° in B. The dihedral angle between the molecular plane of the NO_2 group and the benzene ring is 5.5° in A and 28.9° in B.

In our primary study, we found that intermolecular weak interactions, such as halogen ··· π, π ··· π and H-bonding, play an important role in controlling the stacking structure in the series of [R-BzPy][M(mnt)$_2$] (M = Ni(III), Pt(III)).[5] In **1**, there exist two types of weak interactions in addition to van de Waals intermolecular interactione, *i.e.* H-bonding interaction between H atoms of aryl rings and O atoms of nitryl group, and π ··· π stacking interactions between cations and anions. The H-bonding separation between O(2) and C(14)^{i} (i = 1 + *x*, *y*, *z*) atoms is 3.11 Å, and the corresponding angle O(2) ··· H(14B)^{i}–C(14)^{i} is 118.8°, the distance between O(4) and C(24)^{j} (j = *x*, 1 + *y*, *z*) atoms is 3.18 Å, and the corresponding angle O(4) ··· H(24)^{j}–C(24)^{j} is 137.4°, in accord with literature expectations.[10] The overlapping π ··· π interactions involve the benzene rings C(26^{k})C(27^{k})C(28^{k})C(29^{k})C(30^{k})C(31^{k}), C(26^{j})C(27^{l})C(28^{l})C(29^{l})C(30^{l})C(31^{l}) (k = *x* − 1, *y* + 1, *z* − 1; l = *x*, *y* + 1, *z* − 1) and the conjugated portion of mnt^{2-}. The shorter atom contacts between the overlapped regions are: C(1) ··· C(31^{k}) = 3.46 Å, C(1) ··· C(26^{l}) = 3.57 Å, C(1) ··· C(31^{l}) = 3.54 Å, C(2) ··· C(26^{k}) = 3.56 Å, C(2) ··· C(31^{k}) = 3.49 Å, C(2) ··· C(26^{l}) = 3.50 Å and C(2) ··· C(27^{l}) = 3.58 Å. The weak intermolecular interactions are shown in Fig. 2, with cations and anions forming alternating stacks though both H-bonding and π ··· π stacking interactions, along the direction of the *a*-axis (Fig. 3). Obviously, the stacking pattern of **1** differs from that of the Ni(III) and Pt(III) complexes which show well-separated stacking columns.

Table 2 Selected bond lengths (Å) and bond angles (°) for **1** and **2**.

	1		**2**
Cu(1)–S(1)	2.275(2)	Cu(1)–S(1)	2.257(2)
Cu(1)–S(3)	2.2658(19)	Cu(1)–S(3)	2.276(2)
Cu(1)–S(2)	2.2658(18)	Cu(1)–S(2)	2.255(2)
Cu(1)–S(4)	2.275(2)	Cu(1)–S(4)	2.270(2)
S(1)–Cu(1)–S(2)	91.05(8)	S(1)–Cu(1)–S(2)	90.84(8)
S(1)–Cu(1)–S(3)	88.04(8)	S(1)–Cu(1)–S(3)	90.37(7)
S(1)–Cu(1)–S(4)	178.13(11)	S(1)–Cu(1)–S(4)	176.31(10)
S(2)–Cu(1)–S(3)	179.06(9)	S(2)–Cu(1)–S(3)	178.13(9)
S(2)–Cu(1)–S(4)	89.84(8)	S(2)–Cu(1)–S(4)	89.29(7)
S(3)–Cu(1)–S(4)	91.08(7)	S(3)–Cu(1)–S(4)	89.60(7)

[Br-BzPy]$_2$[Cu(mnt)$_2$] (2). On first inspection, the overall structure of **2** seems to be closely related to that of **1**. The asymmetric unit contains one $[Cu(mnt)_2]^{2-}$ anion and two $[Br\text{-}BzPy]^+$ cations, similarly to **1**. In this complex, the $[Cu(mnt)_2]^{2-}$ anion is a non-planar structure, and the atoms with larger deviations from the S4 plane are: N(2) (0.200 Å), N(3) (0.658 Å), N(4) (0.704 Å), C(4) (0.154 Å), C(5) (0.524 Å), C(6) (0.296 Å), C(7) (0.261 Å), C(8) (0.522 Å). The Cu–S bond lengths and the S–Cu–S bond angles within the five-membered ring are similar to those of **1** and are collected in Table 2. The molecular configurations for the two $[Br\text{-}BzPy]^+$ cations in the asymmetric unit are very different from each other, and the dihedral angles of the pyridine ring and benzene ring with the reference plane C_{Ar}–CH_2–C_{Py} are 80.2, 86.4° for the cation containing the N(5) atom, and 100.4, 4.6° for the cation containing the N(6) atom. Contrary to the situation encountered in **1**, two [Br-BzPy]$_2$[Cu(mnt)$_2$] entities are imposed in a centrosymmetric environment within the cell in **2**. In addition, there are no short contacts between aryl rings of the cation and the conjugated region of the mnt^{2-} ligand unlike in **1**, but there are shorter spaces between Cu, S atoms of the anions and Br atoms of the cations: Br(1) ··· S(2) (1 + *x*, *y*, *z*) = 3.72 Å, Br(1) ··· Cu(1) (1 + *x*,

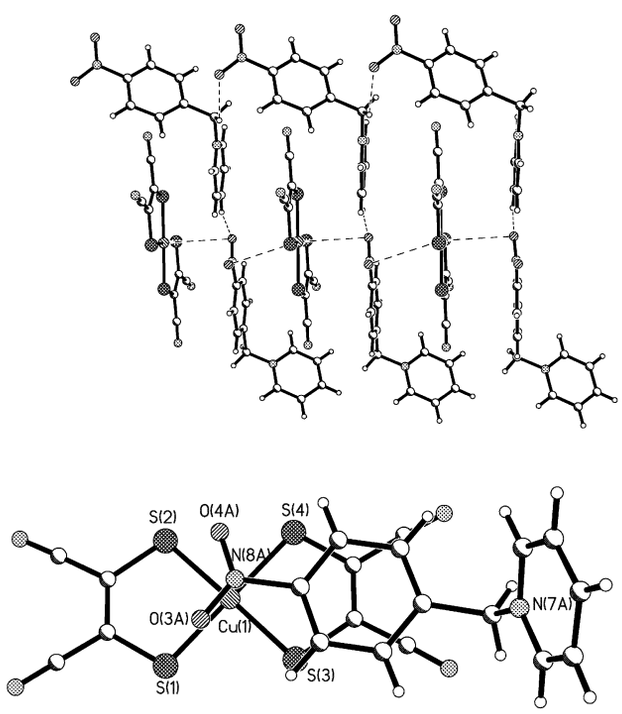

Fig. 2 Side view of the mixed stack alternating anions and cations (top) and π–π stacking interactions between cations and anions (bottom) for **1**.

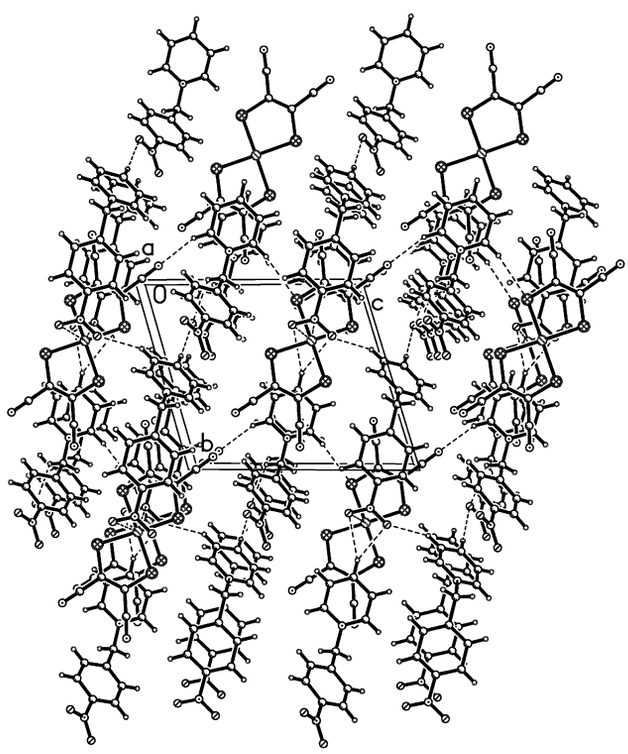

Fig. 3 Perspective view of **1** down the *a*-axis, showing the alternating stacks of anions and cations.

y, z) 3.71 Å, and Br(2) ··· S(2) (1 − x, 1 − y, z) 3.58 Å (as shown in Fig. 4). The stacking pattern of **2** is different from that of **1** (Fig. 5), which shows the side-by-side anion arrangement along the crystallographic b-axis.

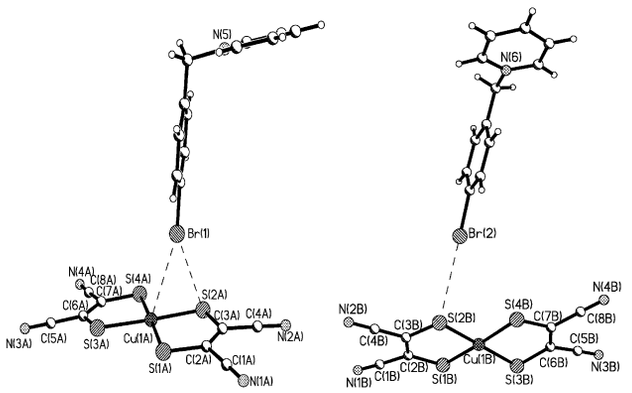

Fig. 4 The weak interactions between cations and anions in **2**.

Ferroelectric properties and theoretical calculations

Stacks of ion-pairs carry an electric dipole,[11] and the corresponding material in the solid state may exhibit ferroelectric behavior in non-centrosymmetric space groups. Ferroelectric behavior in **1**, which crystallises in the non-centrosymmetric space group $P1$, is confirmed by a dielectric hysteresis loop (Fig. 6) at 293 K, and the corresponding parameters are as follows: remnant polarization, $+P_r$ = 0.121 μC cm^{-2}, $-P_r$ = 0.180 μC cm^{-2}; coercive field, $+E_c$ = 0.510 V cm^{-1}, $-E_c$ = 0.491 V cm^{-1}. The dielectric hysteresis loop of **1** shows an irregular shape, which originates from the two electrode surfaces not being parallel. In practice, it is difficult to make the two opposite surfaces of the crystal parallel with each other because the crystals are fragile.

Complex **1** displays a bulk dielectric response due to the correlated alignment of local electric dipoles.[12] To understand the details of the dipole alignment in the solid state, unrestricted density functional theory (DFT) calculations with B3LYP functional and the LANL2DZ basis set were performed on a single unit cell of **1** using the GAUSSIAN 98 program[13] on the SGI 3800 workstation. Taking the mean plane of the nearly-planar $[Cu(mnt)_2]^{2-}$ as the xy plane, the calculated dipole moment in the unit cell were μ_x = −55.4646 D, μ_y = 9.4871 D, μ_z = −5.6287 D, with a total dipole moment of 56.5509 D. Thus there are non-zero electric dipole moments for **1** in the solid state, the main component of which is approximate on the xy plane (the anion molecular plane). For a substance showing ferroelectric properies, spontaneous polarization exists in the ferroelectrics phase, and the spontaneous polarization direction in the unit cell is in agreement with that of the dipole direction for complex **1**.[14] Fig. 7 shows the molecular arrangement in a unit cell and the directions of the inherent dipole moments of pyridinium rings and nitrobenzene rings in the two cations, in which the molecular planes of the anion $[Cu(mnt)_2]^{2-}$ (plane 1), pyridine ring N(5)C(9)C(10)C(11)C(12)C(13) (plane 2) and benzene ring C(27)C(28)C(29)C(30)C(31)C(32)N(8)O(3)O(4)

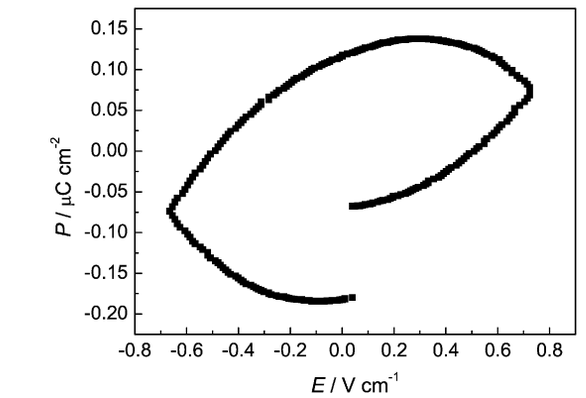

Fig. 6 Dielectric hysteresis loop of **1** at 293 K.

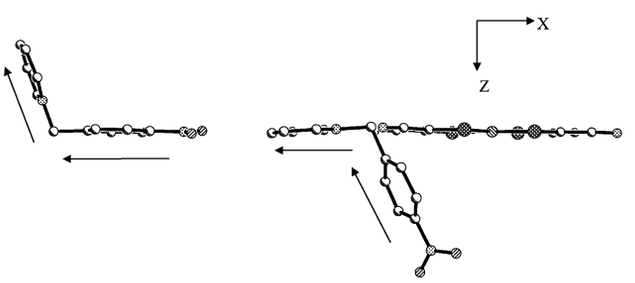

Fig. 7 The relationship of molecular planes between cations and anion in a unit cell (the mean plane of the $[Cu(mnt)_2]^{2-}$ as the xy plane), and arrows indicating the inherent dipole directions in benzene rings and pyridinium rings for **1**.

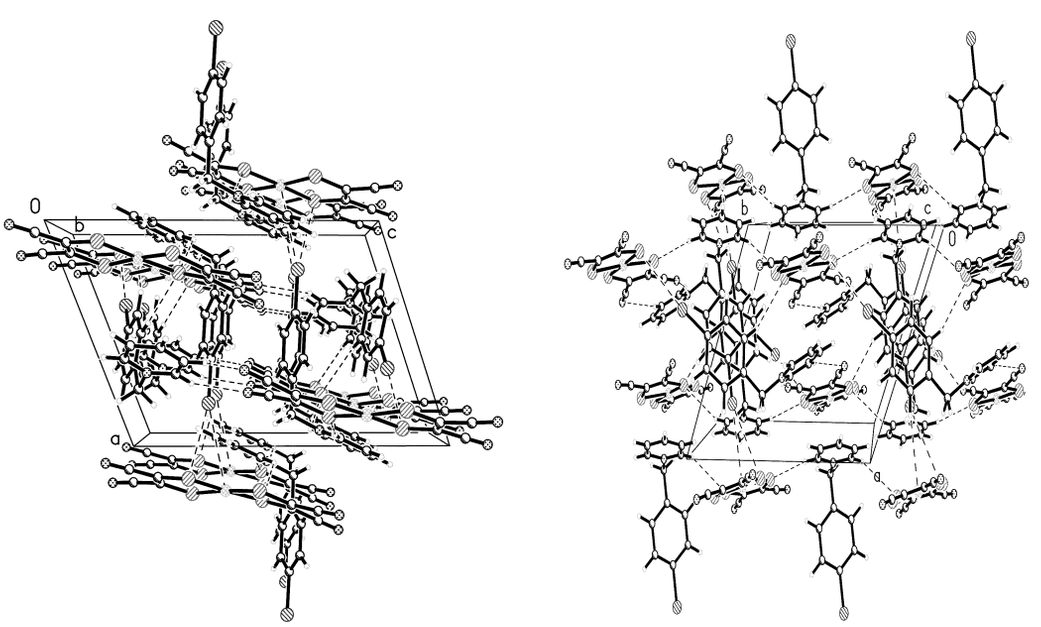

Fig. 5 Stacking diagrams showing the side-by-side arrangement of anions in **2**.

(plane 3) are almost parallel with each other (the dihedral angles between planes 1 and 2 is 4.34(15)°, planes 1 and 3 is 0.89(8)°, planes 2 and 3 is 4.40(17)°). The spontaneous polarization, $\boldsymbol{P}_s$, in a unit cell can be described by eqn. (1):

$$\boldsymbol{P}_s = \boldsymbol{P}_e + \boldsymbol{P}_i + \boldsymbol{P}_d \quad (1)$$

where $\boldsymbol{P}_e$, $\boldsymbol{P}_i$ and $\boldsymbol{P}_d$ denote the polarizations arising from electronic displacement, ionic displacement and dipole–dipole interaction, respectively. In this case, the polarization in the direction perpendicular to the *xy* plane (anion molecular plane) is essentially $\boldsymbol{P}_d + \boldsymbol{P}_e$ (see Fig. 7), and smaller than that on the *xy* plane, so it can be concluded that the polarization on the *xy* plane is mainly resulting from $\boldsymbol{P}_i$. Obviously, $\boldsymbol{P}_i$ is larger than $\boldsymbol{P}_d + \boldsymbol{P}_e$. In addition, it is possible that relative displacement between anions and cations can be easily induced by an external electric field because there are only weak van de Waals interactions between cations and anions apart from electrostatic interactions. Therefore, the possible microscopic mechanism of ferroelectric behavior for complex **1** is mainly based on ion displacement. Normally, spontaneous polarization is always accompanied by lattice deformation, so-called spontaneous deformation, and the spontaneous polarization increases as the temperature decreases, so variable temperature structural determination can also give some information about spontaneous deformation.[14] The temperature dependence of the relative cell parameters, which are defined as a cell parameter measured at T/K divided by the corresponding cell parameter at 376 K [$P_{cell}(T)/P_{cell}(376\ K)$] for complex **1**, was obtained from powder X-ray patterns and fitted by the Powdercell 2.3 program[15] as shown in Fig. 8. During cooling, the cell dimensional change is highly anisotropic, the *a*-, *b*- and *c*-axes and γ decrease, but β and α increase, which can indicate the trend of the spontaneous deformation.

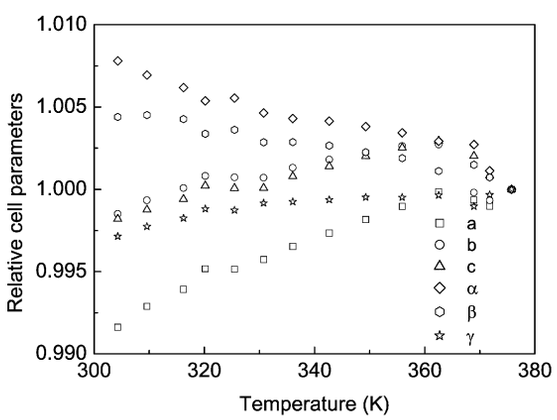

Fig. 8 The temperature dependence of the relative cell parameters for **1**, and the relative cell parameters at T/K defined as $RP_{cell}(T) = P_{cell}(T)/P_{cell}(376\ K)$.

Thermodynamic properties

The power-compensated DSC trace of **1** in the temperature range 323–443 K (50–170 °C) is shown in Fig. 9. The result revealed two endothermic peaks, the strong peak at 416.44 K corresponds to melting of this complex (melting point of **1** is 415 ± 0.5 K), while the weak peak at 377.0 K indicates the ferroelectric–paraelectric phase transition, and the Curie temperature, T_c, is thus 377.0 K. The enthalpy change of the ferroelectric–paraelectric phase transition, ΔH = 763.5 J mol^{-1} is obtained based on the area of the peak, and this indicates the ferroelectric–paraelectric transition is first-order.[16]

EPR spectra and magnetic susceptibilities

The EPR spectra of polycrystalline samples for **1** and **2** at room temperature show an intense signal (Fig. 10). For **1**, the spectrum exhibits characterized axial g tensors with $g_{||}$ of 2.09 and $g_{\perp}$ of 2.02, which are agreement with the results of the literature;[9] $g_{||} > g_{\perp}$ indicates the ground state of copper ion is $d_{x^2-y^2}$.

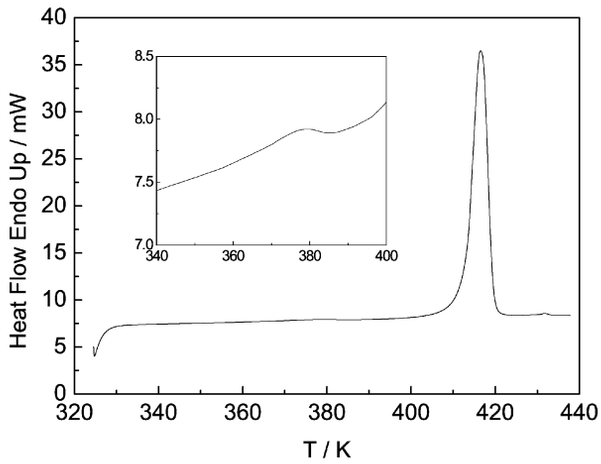

Fig. 9 The DSC curve of DSC of **1**

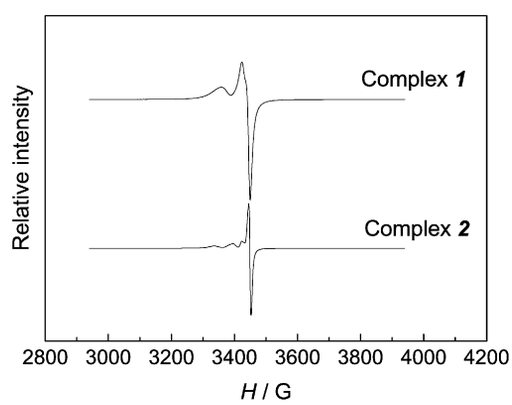

Fig. 10 EPR spectra of polycrystalline samples of **1** and **2** (at room temperature).

For **2**, the room-temperature polycrystalline EPR spectrum is different from that of **1**, and displays the typical four-line patterns expected for coupling of an electron to the spin 3/2 copper(II) nucleus.[17] Three of the four parallel hyperfine features are well resolved while the fourth one at high field is overlapped with the $g_{\perp}$ signal. The g and A tensors are: $g_{||}$ = 2.05, $g_{\perp}$ = 2.03, $A_{||} = 40.6 \times 10^{-4}$ cm^{-1}.

The magnetic susceptibilities were studied in the range of 1.89–260 K for **1** and 1.9–250 K for **2**. Correction for the diamagnetism of the two complexes, estimated from Pascal's constants were -2.1×10^{-4} emu mol^{-1} for **1** and -2.3×10^{-4} emu mol^{-1} for **2**.

For **1**, the effective magnetic moment decreases from 1.76 μ_B at 260 K to 1.65 μ_B at 1.89 K, indicating antiferromagnetic coupling between the nearest-neighbor Cu(II) ions. The magnetic behavior may be interpreted in terms of the Curie–Weiss law:

$$\chi_m = C/(T - \theta) \quad (2)$$

where $C = Ng^2\mu_B^2S(S + 1)/3k_B$, and the other symbols have their usual meanings. The plots (Fig. 11) of the molar magnetic susceptibility corrected for diamagnetism *versus* temperature are fitted using eqn. (2) to give $\theta = -0.580$ K, $C = 0.442$ emu K mol^{-1} and $R = 5.0 \times 10^{-5}$ (R is the agreement factor defined as $\Sigma_i[(\chi_m)_{obs}(i) - (\chi_m)_{calc}(i)]^2/\Sigma_i[(\chi_m)_{obs}(i)]^2$); the g value obtained from the Curie–Weiss constant C is 2.17, which is slightly larger

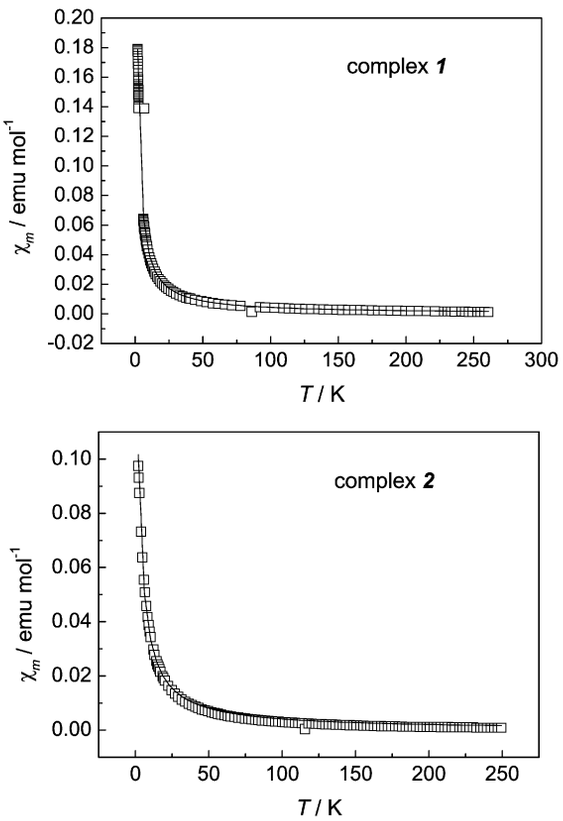

Fig. 11 Plots of χ_m *versus* T for **1** and **2** (□ experimental values, — best fit curve).

than the average g value measured by EPR (2.04). The small minus value of θ reveals the antiferromagnetic interaction between adjacent Cu(II) ions is very weak, which is also illustrated by the absence of a maximum in the χ_m *versus* T curve above 1.89 K.

The magnetic behavior of **2** exhibits an antiferromagnetic exchange interaction between adjacent Cu(II) ions, which is similar to that of **1**. The best fit for the temperature-dependent magnetic susceptibility in the temperature range 1.9–250 K, using eqn. (1), gives $\theta = -2.167$ K, $C = 0.419$ emu K mol^{-1} and $R = 4.2 \times 10^{-5}$; the g value obtained from the Curie–Weiss constant C is 2.11, which is also slightly larger than the average g value measured by EPR (2.04).

Conclusion

In summary, the crystal structures of two ion-pair complexes, which consist of 1-(4′-R-benzyl)pyridinium (R = NO_2 (**1**), Br (**2**)) and bis(maleonitriledithiolato)cuprate(II), have been determined, and the results reveal that the stacking patterns for these two complexes are different from the complexes of Ni(III) and Pt(III), in that the anions and cations do not form well-separated stacking columns. The packing models in **1** and **2** are also different from each other although the difference between the molecular structures of these complexes is only the substituent of benzene, and the difference may originate from the intermolecular interactions between cations and anions. Complex **1** crystallized in the $P1$ space group, its ferroelectric property was measured, which shows a hysteresis loop and a T_c of 377 K; quantum chemistry calculation further indicate there is a non-zero dielectric dipole in the unit cell. The possible mechanism of ferroelectric behavior for complex **1** is mainly based on the ion displacement in terms of the analysis of the crystal structure and quantum chemistry calculations. To our best knowledge, this complex is first example with ferroelectric property. Further investigations of the ferroelectric property of **1** are in progress. Our results suggest a possibility that a new ferroelectric material family might be discovered by rationally designing ion-pair complexes with dipole moments, and we are actively pursuing this line of research.

Acknowledgements

We are grateful for the financial support of the Ministry of Science and Technology of China (NKBRSF-G19990646), the National Natural Science Foundation (No. 29771017, No. 29831010, No. 20171001 and No. 20103004), and the Station Education Commission of China. We also give many thanks to Prof. Dai Q. P. and Ms. Yuan Z. R. of DSC Lab in the Center of Analysis and Determination of Nanjing University for determining DSC data.

References

1 (*a*) R. Kato, *Bull. Chem. Soc. Jpn.*, 2000, **73**, 515; (*b*) A. T. Coomber, D. Beljonne, R. H. Friend, J. L. Brédas, A. Charlton, N. Robertson, A. E. Underhill, M. Kurmoo and P. Day, *Nature*, 1996, **380**, 144; (*c*) T. Manabe, T. Kawashima, T. Ishii, H. Matsuzaka, M. Yamashita, T. Mitani and H. Okamoto, *Synth. Met.*, 2001, **116**, 415; (*d*) J. H. Wei, J. Q. Zhao, D. S. Liu, S. J. Xie, L. M. Mei and J. Hong, *Synth. Met.*, 2001, **122**, 305; (*e*) W. Fujita and K. Awaga, *Science*, 1999, **286**, 261; (*f*) T. Sugano, *Polyhedron*, 2001, **20**, 1285 and references therein; (*g*) J. Kommandeur and J. G. Vegter, *Mol. Cryst. Liq. Cryst.*, 1975, **30**, 11; (*h*) A. Kosaki, M. Sorai, H. Suga and S. Seki, *Bull. Chem. Soc. Jpn.*, 1977, **50**, 810; (*i*) A. Caneschi, D. Gatteschi, N. Lalioti, C. Sangregorio, R. Sessoli, G. Venturi, A. Vingingni, A. Rettori, M. G. Pini and M. A. Novak, *Angew. Chem., Int. Ed.*, 2001, **40**, 1760; (*j*) B. Wolf, S. Zherlitsyn, S. Schmidt and B. Lüthi, *Phys. Status Solidi A*, 2002, **189**, 389; (*k*) M. Mitsumi, K. Kitamura, A. Morinaga, Y. Ozawa and M. Kobayashi, *Angew. Chem., Int. Ed.*, 2002, **41**, 2767; (*l*) T. Lorenz, M. Hofmann, M. Grüninger, A. Freimuth, G. S. Uhrig, M. Dumm and M. Dressel, *Nature*, 2002, **418**, 614.
2 J. Nishijo, E. Ogura, J. Yamaura, A. Miyazaki, T. Enoki, T. Takano, Y. Kuwatani and M. Iyoda, *Solid State Commun.*, 2000, **116**, 661.
3 A. E. Pullen, C. Faulmann, K. I. Pokhodnya, P. Cassoux and M. Tokumoto, *Inorg. Chem.*, 1998, **37**, 6714.
4 M. L. Allan, A. T. Coomber, I. R. Marsden, J. H. F. Martens, R. H. Friend, A. Charlton and A. E. Underhill, *Synth. Met.*, 1993, **55–57**, 3317.
5 (*a*) X. M. Ren, C. S. Lu, Y. J. Liu, H. Z. Zhu, H. F. Li, C. J. Hu and Q. J. Meng, *Transition Met. Chem.*, 2001, **26**, 136; (*b*) X. M. Ren, H. F. Li, P. H. Wu and Q. J. Meng, *Acta Crystallogr., Sect. C*, 2001, **57**, 1022; (*c*) X. M. Ren, Y. C. Chen, C. He and S. Gao, *J. Chem. Soc., Dalton Trans.*, 2002, 3915; (*d*) X. M. Ren, Q. J. Meng, Y. Song, C. J. Hu, C. S. Lu and X. Y. Chen, *Inorg. Chem.*, 2002, **41**, 5686; (*e*) J. L. Xie, X. M. Ren, Y. Song, Y. Zou and Q. J. Meng, *J. Chem. Soc., Dalton Trans.*, 2002, 2868; (*f*) J. L. Xie, X. M. Ren, Y. Song, W. J. Tong, C. S. Lu, Y. G. Yao and Q. J. Meng, *Inorg. Chem. Commun.*, 2002, **5**, 395; (*g*) J. L. Xie and X. M. Ren, *Chem. Commun.*, 2002, 2346; (*h*) X. H. Zhu, X. Z. You, X. M. Ren, W. L. Tan, W. Dai, S. S. S. Raj and H. K. Fun, *Chem. Lett.*, 2000, 472; (*i*) X. M. Ren, Q. J. Meng, Y. Song, C. S. Lu, C. J. Hu, X. Y. Chen and Z. L. Xue, *Inorg. Chem.*, 2002, **41**, 5931; (*j*) J. L. Xie, X. M. Ren, C. He, Z. M. Gao, Y. Song, Q. J. Meng and R. K. Kremer, *Chem. Phys. Lett.*, 2003, **369**, 41.
6 (*a*) A. Davison and H. R. Holm, *Inorg. Synth.*, 1967, **10**, 8; (*b*) S. B. Bulgarevich, D. V. Bren, D. Y. Movshovic, P. Finocchiaro and S. Failla, *J. Mol. Struct.*, 1994, **317**, 147.
7 A. Simon, *J. Appl. Crystallogr.*, 1970, **3**, 11.
8 G. M. Sheldrick, SHELXTL, Structure Determination Software Programs, Version 5.10. Bruker Analytical X-ray Systems Inc., Madison, WI, USA, 1997.
9 K. W. Plumlee, B. M. Hoffman and J. A. Ibers, *J. Chem. Phys.*, 1975, **63**, 1926.
10 L. Turi and J. J. Dannenberg, *J. Am. Chem. Soc.*, 1994, **116**, 8714.
11 (*a*) S. Horiuchi, Y. Okimoto, R. Kumai and Y. Tokura, *J. Am. Chem. Soc.*, 2001, **123**, 665; (*b*) M. Le Cointe, M. H. Lemée-Cailleau, H. Cailleau, B. Toudic, L. Toupet, G. Heger, F. Moussa, P. Schweiss, K. H. Kraft and N. Karl, *Phys. Rev. B*, 1995, **51**, 3374.
12 A. P. Ramirez, M. A. Subramanian, M. Gardel, G. Blumberg, D. Li, T. Vogt and S. M. Shapiro, *Solid State Commun.*, 2000, **115**, 217.
13 GAUSSIAN 98, Revision A.11: M. J. Frisch, G. W. Trucks, H. B. Schlegel, G. E. Scuseria, M. A. Robb, J. R. Cheeseman, V. G. Zakrzewski, J. A. Montgomery, Jr., R. E. Stratmann, J. C. Burant,

S. Dapprich, J. M. Millam, A. D. Daniels, K. N. Kudin, M. C. Strain, O. Farkas, J. Tomasi, V. Barone, M. Cossi, R. Cammi, B. Mennucci, C. Pomelli, C. Adamo, S. Clifford, J. Ochterski, G. A. Petersson, P. Y. Ayala, Q. Cui, K. Morokuma, P. Salvador, J. J. Dannenberg, D. K. Malick, A. D. Rabuck, K. Raghavachari, J. B. Foresman, J. Cioslowski, J. V. Ortiz, A. G. Baboul, B. B. Stefanov, G. Liu, A. Liashenko, P. Piskorz, I. Komaromi, R. Gomperts, R. L. Martin, D. J. Fox, T. Keith, M. A. Al-Laham, C. Y. Peng, A. Nanayakkara, M. Challacombe, P. M. W. Gill, B. Johnson, W. Chen, M. W. Wong, J. L. Andres, C. Gonzalez, M. Head-Gordon, E. S. Replogle and J. A. Pople, Gaussian, Inc., Pittsburgh, PA, 2001.

14 T. Mitsui, I. Tatsuzaki and E. Nakamura, (translated by Y. Ishibashi), *An Introduction to the Physics of Ferroelectrics*, Gordon and Breach Science Publishers, New York, NY, 1976.

15 W. Kraus and G. Nolze, Powdercell for windows version 2.3, BAM, Federal Institute for Materials Research and Testing, Berlin, 1999.

16 (*a*) I. Hatta and S. Nakayama, *Thermochim. Acta*, 1998, **318**, 21; (*b*) R. Jakubas, P. Clapala, A. Pietraszko, J. Zaleski and J. Kusz, *J. Phys. Chem. Solids*, 1998, **59**, 1309; (*c*) T. Tang, K. M. Gu, Q. Q. Cao, D. H. Wang, S. Y. Zhang and Y. W. Du, *J. Magn. Magn. Mater.*, 2000, **222**, 110.

17 (*a*) P. Kamatchi and M. Kandaswamy, *Polyhedron*, 1998, **17**, 1397; (*b*) G. A. McLachlan, G. D. Fallon, R. L. Martin and L. Spiccia, *Inorg. Chem.*, 1995, **34**, 254; (*c*) C. Fraser and B. Bosnich, *Inorg. Chem.*, 1994, **33**, 338.